

1 International Journal of Wavelets, Multiresolution
 and Information Processing
 3 Vol. 2, No. 4 (2004) 1–20
 © World Scientific Publishing Company



5 **EMPIRICAL MODE DECOMPOSITIONS AS DATA-DRIVEN**
WAVELET-LIKE EXPANSIONS

7 PATRICK FLANDRIN
 9 *Laboratoire de Physique (UMR CNRS 5672), École Normale Supérieure de Lyon*
46, allée d'Italie 69364 Lyon Cedex 07, France
flandrin@ens-lyon.fr

11 PAULO GONÇALVÈS*
 13 *INRIA Rhône-Alpes*
paulo.goncalves@inria.fr

Received

15 Huang's data-driven technique of Empirical Mode Decomposition (EMD) is applied to
 17 the versatile, broadband, model of fractional Gaussian noise (fGn). The experimental
 19 spectral analysis and statistical characterization of the obtained modes reveal an equiva-
 21 lent filter bank structure which shares most properties of a wavelet decomposition in the
 same context, in terms of self-similarity, quasi-decorrelation and variance progression.
 Furthermore, the spontaneous adaptation of EMD to "natural" dyadic scales is shown,
 rationalizing the method as an alternative way for estimating the fGn Hurst exponent.

Keywords: Empirical Mode Decomposition; wavelets; fractional Gaussian noise.

23 AMS Subject Classification: 42C40, 42C99, 41A46, 60G18

1. Introduction

25 Empirical Mode Decomposition (EMD) has been recently pioneered by Huang
 27 *et al.*³ for adaptively decomposing signals in a sum of "well-behaved" AM–FM
 29 components. The technique has already been applied with success in a host of
 applications^{2,3,9,13,16} but, albeit quite simple in its principle, it lacks theoretical
 31 fundamentals. Indeed, EMD is basically the output of an iterative algorithm: as
 such, it admits no analytical definition and, up to now, the only way of better
 understanding the technique has been to resort to extensive numerical simulations
 33 in well-controlled situations. The present study adopts this perspective, and its
 main objective is to get a detailed statistical knowledge of the EMD behavior when
 it is applied to broadband noise.

*On leave at IST-ISR, Av. Rovisco Pais, 1049–001 Lisbon, Portugal.

2 *P. Flandrin & P. Gonçalves*

1 More precisely, the paper is organized in two main parts. In the first part
 2 (Sec. 2), basics of EMD are presented, the algorithm is described, some exam-
 3 ples are given and (dis-)similarities with wavelet decompositions are qualitatively
 4 underlined. In the second part (Sec. 3), EMD is specifically applied to the versatile,
 5 broadband, model of fractional Gaussian noise (fGn), evidencing a (spontaneous)
 6 decomposition resembling those involved in wavelet decompositions in the same
 7 context. Statistical properties of EMD modes are investigated further in terms
 8 of zero-crossings, marginal statistics and variance-covariance, suggesting an EMD-
 9 based estimation of the fGn Hurst exponent which is quantitatively compared to
 10 the more classical wavelet-based approach. Some complements to the present study
 11 and suggestions for future works are finally discussed in Sec. 4.

2. Empirical Mode Decompositions

2.1. EMD basics

13 The simplest model for an oscillatory waveform $x(t)$ is given by circular functions
 14 of the type $a \cos 2\pi f_0 t$, or combinations of them. Such “Fourier modes” are of par-
 15 ticular interest in the case of stationary signals and linear systems, since they are
 16 eigenfunctions of linear time-invariant operators. However, many physical situa-
 17 tions are known to undergo nonstationary and/or nonlinear behaviors, thus calling
 18 for more elaborate and more meaningful representations. In this respect, one can,
 19 e.g., think of representing signals in terms of amplitude and frequency modulated
 20 (AM–FM) components such that

$$x(t) = \sum_{k=1}^K a_k(t) \cos \varphi_k(t). \quad (2.1)$$

23 The rationale for such a modelling is to compactly encode possible nonstationari-
 24 ties in a time variation of the amplitudes and frequencies of Fourier-like modes. More
 25 generally, signals may also be generated by nonlinear systems for which oscillations
 26 are not necessarily associated with circular functions, thus suggesting decomposi-
 27 tions of the form

$$x(t) = \sum_{k=1}^K x_k(t), \quad (2.2)$$

29 where the components $x_k(t)$ may present both amplitude variations and non-
 30 harmonic, time-varying, oscillations, while being “independent” of each other in
 31 some way.

32 Empirical Mode Decomposition (EMD)³ is a technique which has been designed
 33 primarily for obtaining representations of this type in the case of signals which are
 34 oscillatory (possibly nonstationary and/or generated by a nonlinear system), in
 35 some automatic, fully data-driven, way. In a nutshell, the starting point of EMD is

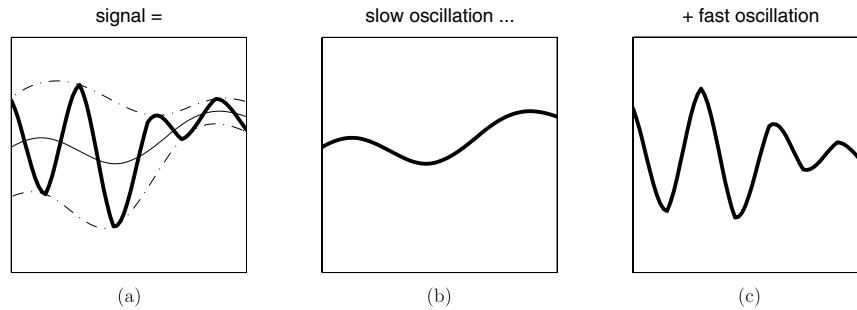


Fig. 1. A schematic illustration of the EMD idea. The original signal (thick line in (a)) is viewed as the superposition of a slow oscillation (b) and a fast oscillation (c), the slow oscillation being obtained as the mean of two envelopes passing through the signal extrema. Once the slow oscillation has been identified, it can be considered as a new signal onto which the same procedure can be applied.

1 to consider oscillatory signals at the level of their local oscillations and to formalize
the idea that:

3 “signal = fast oscillations superimposed to slow oscillations,”

and to iterate on the slow oscillations component considered as a new signal.

5 More precisely (see Fig. 1), if we look at the evolution of a signal $x(t)$ between
two consecutive local extrema (say, two minima occurring at times t_- and t_+), we
7 can heuristically define a (local) “high-frequency” part $\{d(t), t_- \leq t \leq t_+\}$. This
detail $d(t)$ corresponds to the oscillation terminating at the two minima and passing
9 through the maximum which necessarily exists in between them. For the picture to
be complete, we also identify the corresponding (local) “low-frequency” part $m(t)$,
11 or local *trend*, so that we have $x(t) = m(t) + d(t)$ for $t_- \leq t \leq t_+$. Assuming that
this is done in some proper way for all the oscillations composing the entire signal,
13 we get what is referred to as an *Intrinsic Mode Function* (IMF) as well as a *residual*
consisting of all local trends. The procedure can then be applied to this residual,
15 considered as a new signal to decompose, and successive constitutive components
of a signal can therefore be iteratively extracted. The only definition of such a so-
17 extracted “component” is that it is locally (i.e. at the scale of one single oscillation)
in the highest frequency band.

19 Given a signal $x(t)$, the effective algorithm of EMD can therefore be summarized
as the following main loop³:

- 21 (1) identify all extrema of $x(t)$,
- (2) interpolate between minima (respectively maxima), ending up with some “enve-
23 lope” $e_{\min}(t)$ (respectively $e_{\max}(t)$),
- (3) compute the average $m(t) = (e_{\min}(t) + e_{\max}(t))/2$,
- 25 (4) extract the detail $d(t) = x(t) - m(t)$,
- (5) iterate on the residual $m(t)$.

4 *P. Flandrin & P. Gonçalves*

1 In practice, the above procedure has to be refined by a *sifting* process, an inner
 2 loop that iterates steps (1) to (4) upon the detail signal $d(t)$, until this latter can
 3 be considered as zero-mean according to some stopping criterion.^a Once this is
 4 achieved, the detail is considered as the effective IMF, the corresponding residual
 5 is computed and only then, step (5) applies. Eventually, the original signal $x(t)$ is
 6 first decomposed through the main loop as

$$7 \quad x(t) = d_1(t) + m_1(t), \quad (2.3)$$

and the first residual $m_1(t)$ is itself decomposed as

$$9 \quad m_1(t) = d_2(t) + m_2(t), \quad (2.4)$$

so that

$$\begin{aligned} x(t) &= d_1(t) + m_1(t) \\ &= d_1(t) + d_2(t) + m_2(t) \\ &\quad \vdots \\ &= \sum_{k=1}^K d_k(t) + m_K(t). \end{aligned} \quad (2.5)$$

11 By construction, the number of extrema decreases when going from one resid-
 12 ual to the next, thus guaranteeing that the complete decomposition is achieved in
 13 a finite number of steps (typically, K is at most $O(\log_2 N)$ for N data points).
 14 Moreover, the whole decomposition being only based on elementary subtractions,
 15 it obviously allows for a perfect reconstruction of the initial signal $x(t)$, given the
 16 collection of details $\{d_k(t), k = 1, \dots, K\}$ and the residual $m_K(t)$.

17 Modes and residuals have been heuristically introduced on “spectral” argu-
 18 ments, but this must not be considered from a too narrow perspective. First, it
 19 is worth stressing the fact that, even in the case of harmonic oscillations, the high
 20 versus low frequency discrimination mentioned above applies only *locally* and cor-
 21 responds by no way to a pre-determined sub-band filtering. Indeed, selection of
 22 modes rather corresponds to an automatic and adaptive (data-driven) time-variant
 23 filtering. In this direction, Fig. 2 shows an example, where a signal composed of two
 24 AM–FM components significantly overlapping in time and frequency is successfully
 25 decomposed by the method.

26 Another example that puts emphasis on the potentially “non-harmonic” nature
 27 of EMD is given in Fig. 3. In this case, the analyzed signal is composed of a “low
 frequency” triangular waveform to which is superimposed a “middle frequency”
 sine wave whose amplitude is quickly (linearly) decaying and a “high frequency”

^aIt is not the purpose of this paper to address algorithmic issues which have been considered in
 some detail elsewhere.^{3,12} Let us just mention that the main reason for which a proper IMF has to
 be zero-mean is that this is a pre-requisite for its AM–FM demodulation with Hilbert transform
 techniques, a post-processing aspect of EMD that will not be considered here.

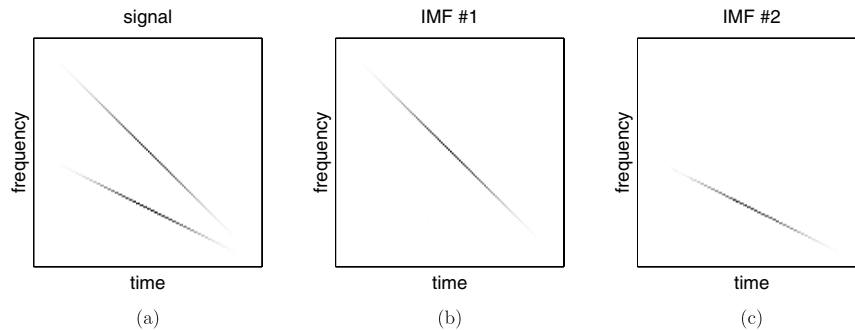


Fig. 2. An example of EMD-based time-variant filtering. A signal consisting in the superposition of two amplitude modulated linear chirps is represented in the time-frequency plane (a), revealing an overlap of the two components in both time and frequency. The EMD of this signal ends up with essentially two IMF's whose time-frequency signatures (b), (c) directly correspond to each of the components. (All time-frequency transforms are reassigned spectrograms.)

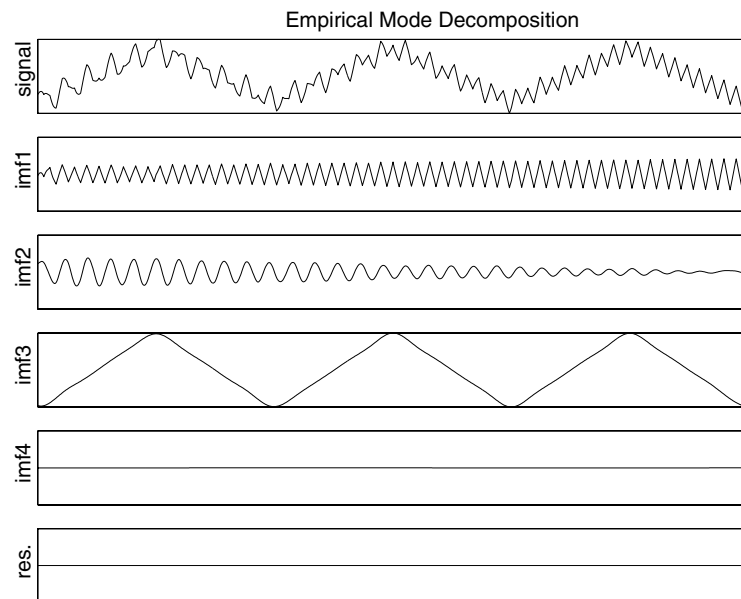


Fig. 3. An example of an EMD-based “non-harmonic” decomposition. The original signal (top diagram) is decomposed into three main components revealing both linear and nonlinear oscillations (one sine wave (IMF 2) and two triangular waveforms (IMFs 1 and 3)), together with possible amplitude modulations.

- 1 triangular waveform whose amplitude is slowly (linearly) growing. Both linear and nonlinear oscillations are effectively identified and separated by EMD, whereas any
- 3 “harmonic” analysis (Fourier, wavelets, ...) would end up in the same context with a much less compact and physically less meaningful decomposition.

1 **2.2. EMD versus wavelets: A qualitative appreciation**

3 The brief EMD description sketched above is somehow reminiscent of wavelet
 4 analysis,¹⁰ at least in the sense that it corresponds to an iterative decomposition
 5 scheme aimed at progressively scrutinizing coarser and coarser scales in a signal.
 6 In parallel with what has been said on the basic idea underlying EMD, we can say
 7 that the starting point of a wavelet decomposition is to formalize the idea that:

8 “signal = high-frequency detail superimposed to low-frequency approximation,”
 9 and to iterate on the approximation considered as a new signal.

10 The way this decomposition is conventionally achieved consists in a repeated
 11 application of two filtering operations. First, a high-pass (respectively low-pass)
 12 filter extracts the detail (respectively approximation) part of the signal by identi-
 13 fying it as the one which lives in the highest (respectively lowest) frequency band.
 14 Second, the very same filters are applied to the approximation considered as a new,
 15 full-band, signal after a decimation by a factor of two. Compared to EMD, the two
 16 main differences are (i) that splitting the signal is achieved, at each step of the
 17 decomposition, on a pre-determined spectral basis, and (ii) that the use of linear
 18 time-invariant filters precludes the possibility of adapting to local variations of the
 19 oscillations.

20 However, wavelet decompositions present the advantage of being based on solid
 21 and well-understood theoretical foundations, and to be equipped with extremely
 22 efficient fast algorithms. This of course contrasts with the present situation of EMD,
 23 whose definition is only given as the output of an algorithm, and which clearly lacks
 from a well-established theory.

3. EMD Analysis of Broadband Noise

24 In order to better compare EMD and wavelet analysis, an empirical way is to resort
 25 to extensive simulations in situations that are already well-documented from the
 26 point of view of wavelets, and which are expected to reveal specific features of EMD
 27 in terms of hierarchical extraction of components in a fluctuating signal. One such
 28 situation is provided by scaling processes for which wavelets are known to be a
 29 naturally fitted analysis tool.¹

31 **3.1. The model of fractional Gaussian noise**

32 Fractional Gaussian noise (fGn)^{4,11} is a generalization of ordinary white noise, and
 33 it is a versatile model for broadband noise dominated by no particular frequency
 34 band. It is intrinsically a discrete-time process, which is expressed as the increment
 35 process of fractional Brownian motion (fBm), the latter being the only self-similar
 36 Gaussian process with stationary increments. As a consequence, the statistical prop-
 37 erties of fGn are entirely determined by its second-order structure, which turns out
 38 to depend only on one single scalar parameter H , referred to as its Hurst expo-
 39 nent. More precisely, $\{x_H[n], n = \dots, -1, 0, 1, \dots\}$ is said to be a fGn of index H

1 (with $0 < H < 1$) if and only if it is a zero-mean Gaussian stationary process whose
autocorrelation sequence $r_H[k] := \mathbb{E}\{x_H[n]x_H[n+k]\}$ reads:

$$3 \quad r_H[k] = \frac{\sigma^2}{2} (|k-1|^{2H} - 2|k|^{2H} + |k+1|^{2H}). \quad (3.1)$$

As is well known, the special case $H = 1/2$ reduces to (discrete-time, uncorrelated) white noise, whereas other values induce nonzero correlations, either negative when $0 < H < 1/2$ or positive when $1/2 < H < 1$ (long-range dependence). Taking the discrete Fourier transform of (3.1), we readily get that the power spectrum density of fGn expresses as:

$$9 \quad \mathcal{S}_H(f) = C \sigma^2 |e^{i2\pi f} - 1|^2 \sum_{k=-\infty}^{\infty} \frac{1}{|f+k|^{2H+1}}, \quad (3.2)$$

with $|f| \leq 1/2$. If $H \neq 1/2$, we have $\mathcal{S}_H(f) \sim C \sigma^2 |f|^{1-2H}$ when $f \rightarrow 0$, making of fGn a convenient model for power-law spectra at low frequencies. From this spectral perspective too, the particular value $H = 1/2$ delineates two domains with contrasted behaviors. In the regime $0 < H < 1/2$, we have $\mathcal{S}_H(0) = 0$ and the spectrum is high-pass. On the contrary, within the range $1/2 < H < 1$, we have $\mathcal{S}_H(0) = \infty$, with a “ $1/f$ ”-type spectral divergence (sometimes referred to as an “infrared” catastrophe). In both situations, it has to be noted that the power-law form of the spectrum, although not exactly verified, is fairly well approximated over most of the Nyquist frequency band. In other words, we have a quasi-linear relation in log–log coordinates:

$$19 \quad \log \mathcal{S}_H(f) \approx (1 - 2H) \log |f| + C \quad (3.3)$$

21 for most frequencies $-1/2 \leq f \leq 1/2$.

3.2. EMD equivalent filter banks

23 We will here report on extensive simulations that have been carried out on fGn
processes, with $H = 0.1, 0.2, \dots, 0.9$. The data length has been typically set to
25 $N = 512$ and, for each value of H , $J = 5000$ independent sample paths of fGn
have been generated via the Wood and Chan algorithm.¹⁴ It is worth mentioning
27 that the present study, whose first results have been proposed in Ref. 6, generalizes
therefore the one conducted independently in Ref. 15 for white noise only ($H = 0.5$)
and will support consistently the findings reported in this case.

EMDs have been computed for all sample paths $\{x_H^{(j)}[n]; n = 1, \dots, N\}$ (with
31 $j = 1, \dots, J$), resulting in a collection of IMFs referred to as $\{d_{k,H}^{(j)}[n]; n =$
33 $1, \dots, N\}$. The maximum number of those IMFs proved to vary from one realization
to the other, but none of them ended up with less than seven modes. This
value has therefore been retained in the study as the maximum considered number
35 of modes ($k = 1, \dots, 7$).

8 *P. Flandrin & P. Gonçalves*

1 Given the so-obtained data set, a spectrum analysis has been carried out mode
 by mode, on the basis of the estimated power spectrum density (PSD) given by

$$\hat{S}_{k,H}(f) := \sum_{m=-N+1}^{N-1} \hat{r}_{k,H}[m] w[m] e^{-i2\pi fm}, \quad |f| \leq 1/2, \quad (3.4)$$

3

where $w[n]$ is a Hamming taper, and

$$\hat{r}_{k,H}[m] = \frac{1}{J} \sum_{j=1}^J \left(\frac{1}{N} \sum_{n=1}^{N-|m|} d_{k,H}^{(j)}[n] d_{k,H}^{(j)}[n + |m|] \right), \quad |m| \leq N - 1 \quad (3.5)$$

5

is the ensemble average (over the J realizations) of the empirical estimates of the autocorrelation function. The result of this spectrum analysis is plotted in Fig. 4,

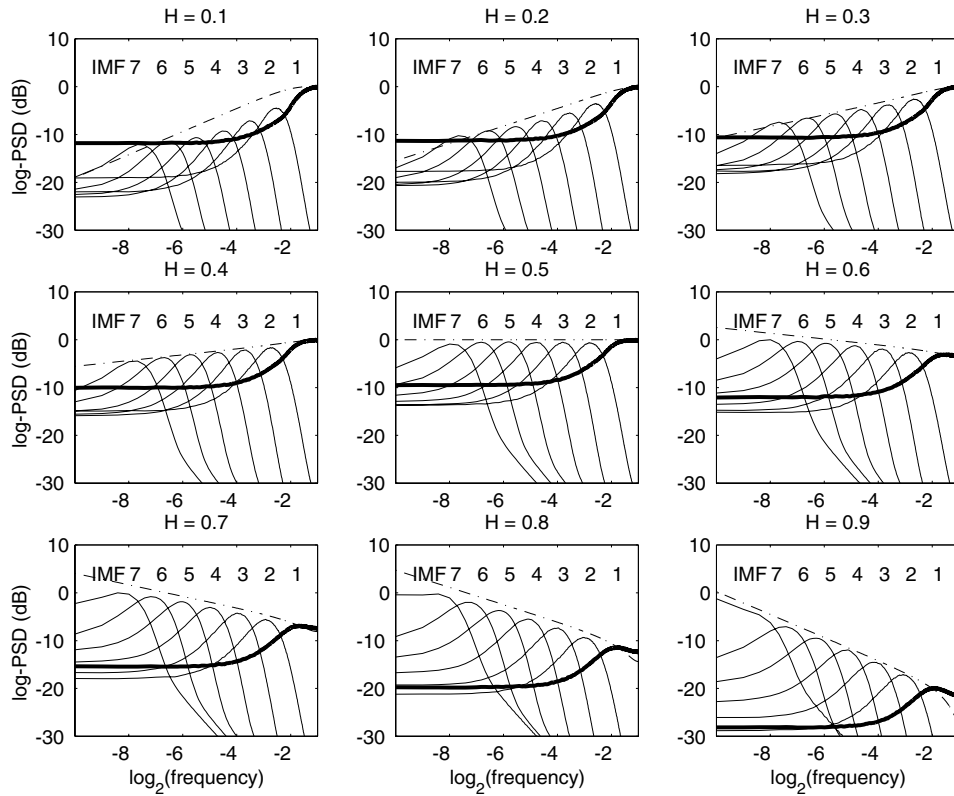


Fig. 4. IMF power spectra in the case of fractional Gaussian noise. The logarithm of the estimated power spectrum densities (log-PSD) is plotted as a function of the logarithm of the normalized frequency for the first 7 IMFs. For each of the nine values of the Hurst exponent H (from 0.1 to 0.9), the spectral estimates have been computed on the basis of 5000 independent sample paths of 512 data points. Theoretical PSDs of the full processes are superimposed as dashed-dotted curves.

1 whose graphs reveal a number of striking features:

- 3 (1) whatever the value of the Hurst exponent H , the behavior of the first IMF
 (thick line) contrasts with that of the other modes in the sense that, in a first
 5 approximation, it presents the characteristics of a high-pass filter, while the
 modes of higher order are much more of a band-pass nature. The (roughly half-
 7 band) high-pass character of the first mode has however to be tempered by the
 fact that the maximum attenuation in the stop-band is no more than 10 dB
 (as compared to the maximum which occurs at the Nyquist frequency $1/2$),
 9 thus corresponding to a non-negligible contribution in the lower half-band in
 “ultraviolet” situations ($H < 1/2$).
- 11 (2) when varying H from 0.1 to 0.9, the spectrum of the last IMF ($k = 7$) is
 progressively turned from band-pass to more and more low-pass, in accordance
 13 with the increasing predominance of low frequencies (“infrared catastrophe”).
- 15 (3) in the same respect, but more generally, the energy balance between the dif-
 ferent modes reflects quite well the behavior of the global spectrum (superim-
 17 posed dashed-dotted curve) described by Eq. (3.2): flat spectrum when $H = 1/2$
 (white noise) and increasing (respectively decreasing) power-law spectrum when
 $H < 1/2$ (respectively $H > 1/2$).
- 19 (4) for the indices $k = 2$ to 6 corresponding to band-pass IMFs, the spectra all
 look quite the same, up to some shifts in abscissa and ordinate, in a surprising
 21 reminiscence of what is currently observed in wavelet decompositions.^{5,10}

23 This last observation prompts one to consider in greater detail how the different
 spectra are related to each other, for a given H . To this end, one can make use
 of the very specific structure of IMFs, according to which all extrema appear as a
 25 succession of minima and maxima with one and only one zero-crossing in between
 them. Measuring the average number of zero-crossings in a mode is therefore a
 27 meaningful way of having access to its mean frequency. A graphical representation
 of the average number of zero-crossings $z_H[k]$ as a function of the IMF number k
 29 is plotted in Fig. 5, suggesting a functional relation of the form:

$$z_H[k] \propto \rho_H^{-k}, \quad (3.6)$$

31 with ρ_H very close to 2.

A more precise check of the relation (3.6) is detailed in Table 1, where the
 33 estimated scaling factor ρ_H is the direct by-product of the slope measurement
 obtained from a linear fit in the semi-log diagram $\log_2 z_H[k]$ versus k , $k = 2$ to 6.

35 Up to a slight dependence on H , one can observe that the average number of
 zero-crossings is, in a first approximation, divided by 2 when going from one IMF
 37 to the next. Based on this result, we can even go further and check for a possible
 self-similarity in the “filter bank” structures of Fig. 5. Restricting to the band-pass
 39 IMFs ($k = 2$ to 6), self-similarity would mean that

$$\mathcal{S}_{k',H}(f) = \rho_H^{\alpha(k'-k)} \mathcal{S}_{k,H}(\rho_H^{k'-k} f) \quad (3.7)$$

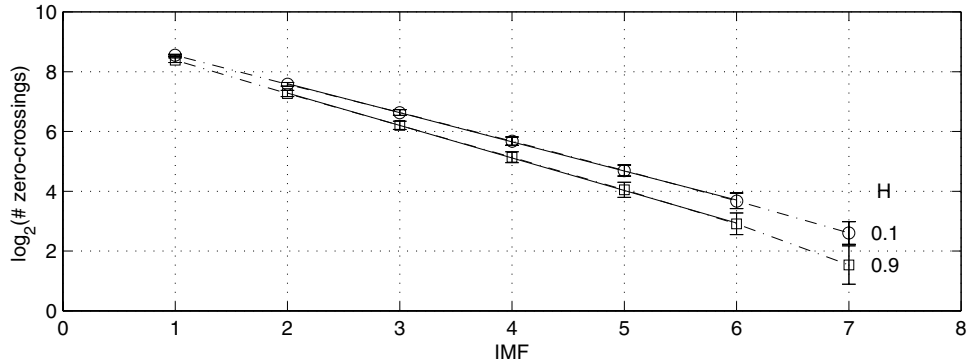


Fig. 5. IMF average number of zero-crossings in the case of fractional Gaussian noise. For a sake of readability, only the curves corresponding to the extreme indices $H = 0.1$ (circles) and $H = 0.9$ (squares) have been plotted in the diagram, all the other considered cases ($H = 0.2, 0.3, \dots, 0.8$) leading to regularly intertwined similar curves (see Table 1). The superimposed full lines correspond to linear fits within the IMF range $k = 2$ to 6.

Table 1. IMF average number of zero-crossings in the case of fractional Gaussian noise.

H	0.1	0.2	0.3	0.4	0.5	0.6	0.7	0.8	0.9
slope	-0.962	-0.972	-0.983	-0.994	-1.01	-1.02	-1.04	-1.06	-1.08
ρ_H	1.95	1.96	1.98	1.99	2.01	2.03	2.06	2.08	2.11

1 for some α and any $k' > k \geq 2$. As a consequence, the power spectra of all IMFs
 2 should collapse onto a single curve, when properly renormalized. Such a collapse via
 3 renormalization can indeed be observed in Fig. 6, obtained with the specific choice
 4 $\alpha = 2H - 1$. Even if some low frequency discrepancies can be observed (especially
 5 when $H < 1/2$), these diagrams support the claim that, in a first approximation,
 EMD acts on fGn as a dyadic filter bank of constant- Q band-pass filters.

7 **3.3. IMF marginal statistics**

8 Although fGn is a Gaussian process, the highly nonlinear structure of EMD cannot
 9 a priori guarantee that fGn IMFs are themselves Gaussian. This, however, turns
 10 out to be true (except for the first, high-pass, mode), as illustrated in Fig. 7. More-
 11 over, not only the modes are Gaussian, but they also evidence a general form of
 12 self-similarity consistent with the one related to the second-order properties dis-
 13 cussed previously: the probability density functions (PDFs) $p(d_{k,H})$ of the different
 14 modes $\{d_{k,H}; k = 2, \dots, 6\}$ can all be deduced one from the other through the
 15 renormalization equation:

$$p(d_{k',H}) = \beta_H^{k'-k} p(\beta_H^{k'-k} d_{k,H}), \quad (3.8)$$

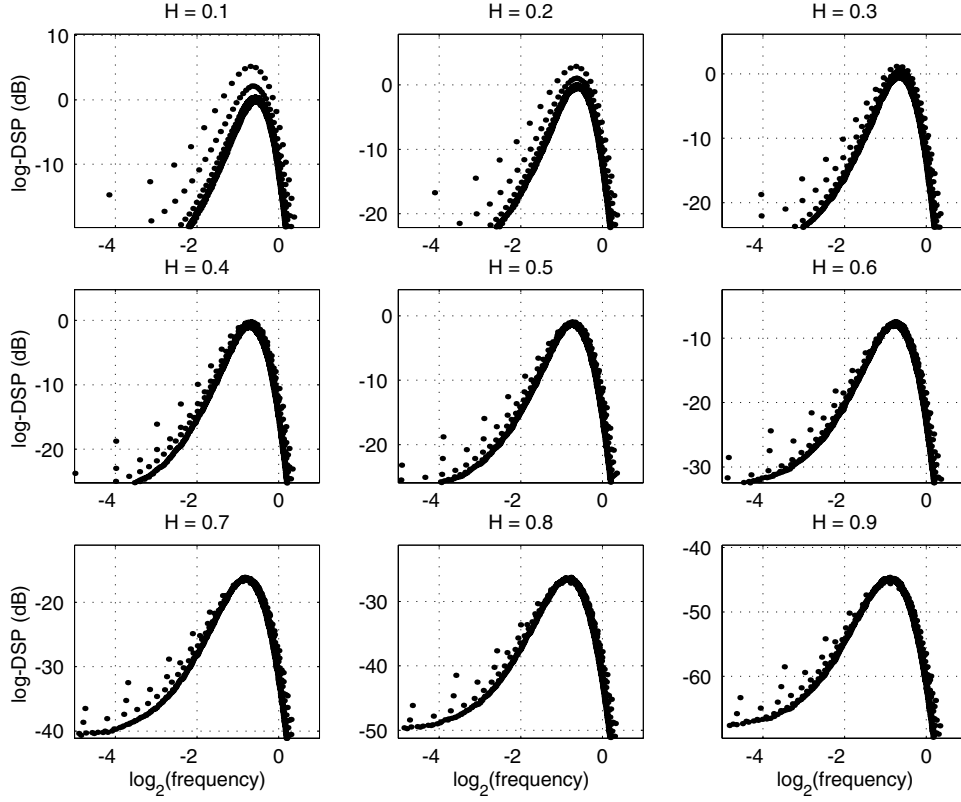


Fig. 6. Renormalized IMF spectra in the case of fractional Gaussian noise. For each value of H , the band-pass IMFs ($k = 2$ to 6) of Fig. 4 are plotted after the renormalization given by Eq. (3.7) with $\alpha = 2H - 1$, and the values of ρ_H listed in Table 1.

1 with $\beta_H := \rho_H^{H-1}$ (the bottom row of Fig. 7 is displayed on a semilogarithmic scale,
 2 so as to better appreciate the Gaussianity of the superimposed IMFs, characterized
 3 by a parabola).

4 As is apparent in the top row of Fig. 7, the PDF of the first IMF is not Gaussian
 5 but bimodal. This shape can be simply justified in the white noise case ($H = 1/2$)
 6 by the following argument. If we label by $p_+(x)$ and $p_-(x)$, respectively, the PDFs of
 7 (Gaussian) white noise maxima and minima, it is easy to show that they express as:

$$p_{\pm}(x) = \left[\frac{1}{2} \pm \left(\frac{1}{2} - \text{erf}(x) \right) \right]^2 \gamma(x), \quad (3.9)$$

8 with

$$\gamma(x) = \frac{1}{\sqrt{2\pi}} e^{-x^2/2} \quad (3.10)$$

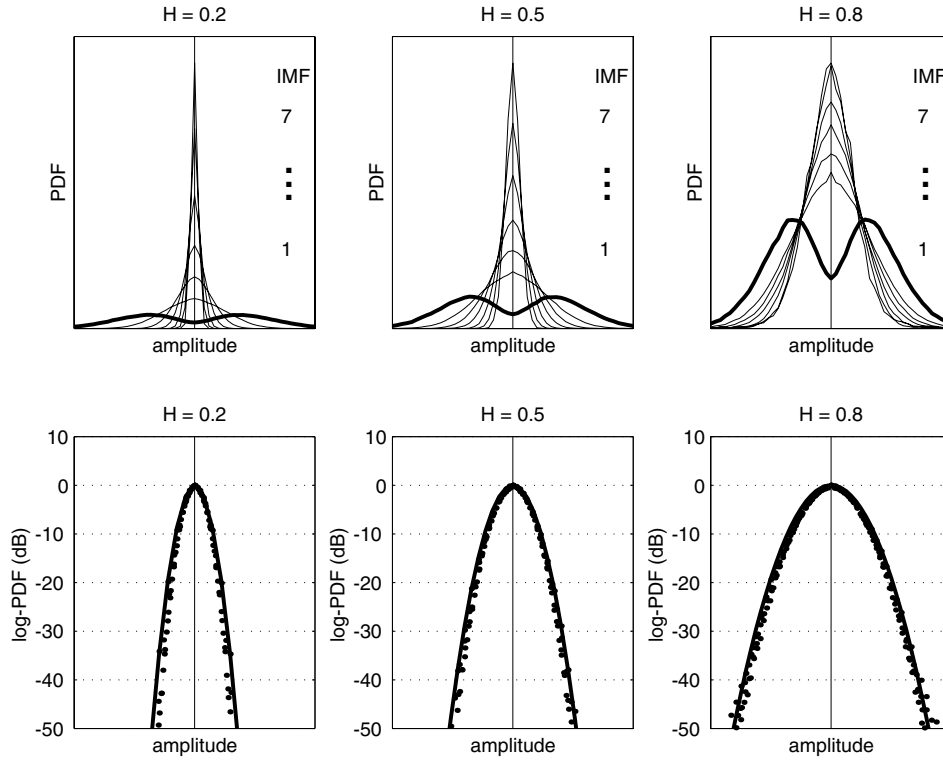


Fig. 7. IMF probability density functions in the case of fractional Gaussian noise. Top row: PDFs of the first 7 IMFs displayed on a linear scale, for three values of H . Bottom row: the corresponding PDFs of the IMFs of indices $k = 2$ to 6 on a semi-logarithmic scale, after the renormalization of Eq. (3.8). Actual values are plotted as dots, while the superimposed thick lines correspond to their Gaussian fits.

1 the normalized Gaussian PDF, and

$$\text{erf}(x) := \int_x^{+\infty} \gamma(\theta) d\theta \quad (3.11)$$

3 the corresponding error function.

5 We have seen that, in a first approximation, the first IMF is a high-pass filtered
 7 version of the input signal. Since, by construction, EMD only retains positive max-
 9 ima and negative minima, this amounts to say that, in the white noise case, the
 PDF of the first IMF is essentially given by $p_*(x) := \max(p_-(x), p_+(x))$. Figure 8
 shows that this simplified model reproduces the main structure of the actual PDF,
 with furthermore a good agreement even in the cases where $H \neq 1/2$.

3.4. EMD-based Hurst exponent estimation

Given the self-similar relation (3.7) for PSDs of the band-pass IMFs, we can deduce
 how variance should evolve as a function of the IMF number. Assuming that (3.7)

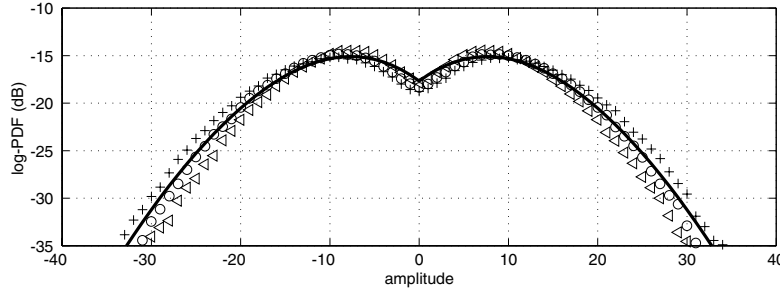


Fig. 8. Log-probability distribution function of the first IMF in the case of fractional Gaussian noise. The full line corresponds to the simplified model in the white noise case $H = 0.5$, whose actual values are plotted as circles. Crosses and triangles correspond, respectively, to the correlated cases $H = 0.2$ and $H = 0.8$. All PDFs have been normalized to be of unit area.

holds for any $k' > k \geq 2$, with $\alpha = 2H - 1$, we have indeed

$$\begin{aligned}
 V_H[k'] &:= \text{var } d_{k',H}[n] \\
 &= \int_{-1/2}^{1/2} \mathcal{S}_{k',H}(f) df \\
 &= \rho_H^{\alpha(k'-k)} \int_{-1/2}^{1/2} \mathcal{S}_{k,H}(\rho_H^{k'-k} f) df \\
 &= \rho_H^{(\alpha-1)(k'-k)} V_H[k],
 \end{aligned} \tag{3.12}$$

1 thus leading to

$$V_H[k] = C \rho_H^{2(H-1)k}. \tag{3.13}$$

3 The IMF variance is therefore expected to be an exponentially decreasing function of the IMF index, with a decay rate which is a simple linear function of the
5 Hurst exponent H . An experimental evidence for this behavior is reported in Fig. 9, where the (energy-based) empirical variance estimate

$$7 \quad \hat{V}_H[k] := \frac{1}{J} \sum_{j=1}^J \left(\frac{1}{N} \sum_{n=1}^N (d_{k,H}^{(j)}[n])^2 \right) \tag{3.14}$$

has been plotted as a function of the index k in a semi-log diagram (in base 2).
9 In accordance with the logarithmically linearized version of (3.13), it appears that straight lines can be fitted to the different curves, with a slope κ_H such that the
11 estimated Hurst exponent \hat{H} reads

$$\hat{H} = 1 + \frac{\kappa_H}{2}. \tag{3.15}$$

13 However, it has to be noticed that the predicted relationship (3.13) only holds for IMF indices $k > 1$, with furthermore an increased discrepancy for smaller H 's
15 (typically, the model reasonably fits the data for $H > 1/4$).

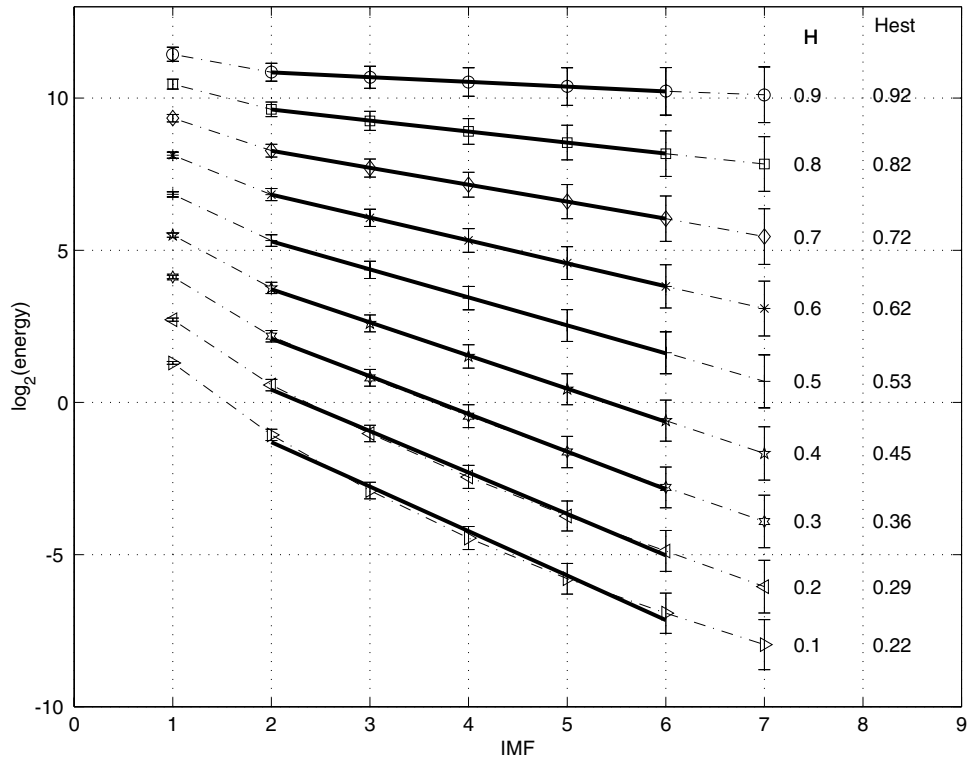


Fig. 9. Estimated IMF \log_2 -variance in the case of fractional Gaussian noise. The actual values of the empirical (energy-based) variance estimates are reported in dotted lines for the different values of the Hurst exponent H , together with error bars corresponding to the standard deviations associated with the 5000 realizations run in the study. The mean value of the estimated Hurst exponents are also given, based on weighted linear fits within the IMF indices range $k = 2$ to 6. For a sake of better readability, all curves have been arbitrarily shifted along the vertical axis to avoid overlapping.

1 **3.5. EMD versus wavelets: A quantitative comparison**

3 In order to better appreciate the possibility of estimating H from a slope in a
 4 diagram “log-energy versus IMF index,” and moreover to compare with wavelet-
 5 based techniques, it is important to not only consider the variance evolution through
 6 modes, but also the possible correlations which may exist within modes and between
 7 them. In fact, it is well known that one of the main features of dyadic wavelet
 8 decompositions (WD) is to approximately decorrelate most processes (even those
 9 with slowly-decaying correlations such as long-range dependent processes, e.g., fGn
 10 with $H > 1/2$), thanks to a tuning parameter which is the number of vanishing
 11 moments of the analyzing mother wavelet.¹ No such tuning parameter exists for
 EMD, and it is worth investigating the resulting correlation structure when applied
 to fGn.

1 To do so, two approaches have been followed. In the first one, we considered a
 2 mere generalization of the previous variance study by computing, for each value of
 3 the Hurst exponent H , the full variance-covariance matrix defined by

$$C_H[k, k'] := \mathbb{E} d_{k,H}[n] d_{k',H}[n]. \quad (3.16)$$

5 From a practical point of view, this quantity has been estimated by

$$\hat{C}_H[k, k'] := \frac{1}{J} \sum_{j=1}^J \left(\frac{1}{N} \sum_{n=1}^N d_{k,H}^{(j)}[n] d_{k',H}^{(j)}[n] \right) \quad (3.17)$$

7 on the basis of 100 independent realizations, for a data size $N = 2048$ and IMF
 8 indices k and k' varying from 1 to 6. Figure 10 presents the obtained normalized
 9 result $\hat{C}_H[k, k']/\hat{C}_H[1, 1]$. As expected, one recovers along the main diagonal (i.e.
 10 for $k = k'$) the behavior reported in Fig. 9, since $\hat{C}_H[k, k] = \hat{V}_H[k]$. The new feature
 11 is that the estimated covariance falls off quickly when moving away from the main
 12 diagonal, thus indicating a low level of inter-modes correlation. This observation
 13 does not apply however to the first IMF which evidences (in the first row and the
 14 first column) a non-negligible amount of correlation with higher-order modes, in
 15 clear accordance with the specific low-pass tail reported in Fig. 4. In good agreement
 16 with Fig. 4 too, we can see that correlations induced by the first IMF are enhanced
 17 for low values of H , i.e. those for which the contribution of IMF 1 prevails at low
 frequencies.

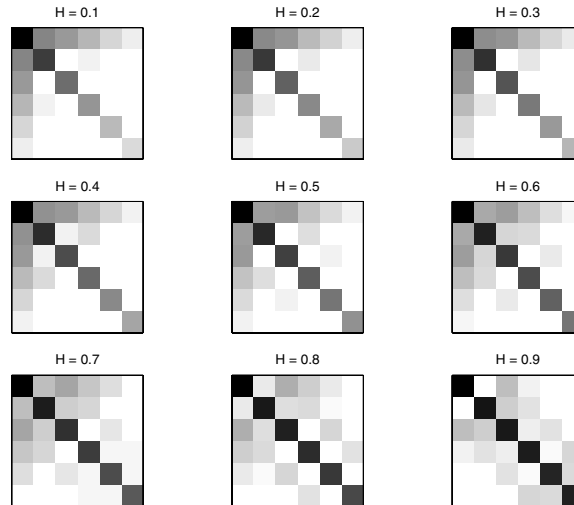


Fig. 10. Estimated IMF variance-covariance matrix in the case of fractional Gaussian noise. For each value of the Hurst exponent H , the graph displays the quantity $|\hat{C}_H[k, k']/\hat{C}_H[1, 1]|$ on a logarithmic gray scale with a dynamic range of 10 dB, IMF indices $1 \leq k, k' \leq 6$ running from top to right and from top to bottom.

1 In a second approach, we focused on band-pass IMFs only ($k > 1$) and evaluated
the two-dimensional correlation function

$$3 \quad D_H[k', n'] := \mathbb{E} d_{k,H}[n] d_{k+k',H}[n+n'] \quad (3.18)$$

by means of the averaged empirical estimate

$$5 \quad \hat{D}_H[k', n'] := \frac{1}{J} \sum_{j=1}^J \left(\frac{1}{NK} \sum_{k=2}^{K-|k'|} \sum_{n=1}^{N-|n'|} d_{k,H}^{(j)}[n] d_{k+|k'|,H}^{(j)}[n+|n'|] \right), \quad (3.19)$$

7 with $|n'| \leq N - 1$ and $|k'| \leq K - 2$, where K stands for the largest IMF
index minus 1, so as to disregard the residual. The result of this two-dimensional
9 correlation function of the full IMF matrix, considered as a two-dimensional field,
is displayed in Fig. 11.

11 As for detail sequences at different scales in wavelet decompositions, the graph
evidences that modes with different indices are almost uncorrelated. The only
13 significant values of $\hat{D}_H[k', n']$ correspond to $k' = 0$, i.e. to intra-scale correlations,
with a correlation decay which becomes slower as H is increased.

15 In terms of estimation of the Hurst exponent H , based on the assumed relation
(3.15) with the slope κ_H deduced from (3.14), the consequences of this behavior are
twofold. First, because of the nonzero intra-scale correlations, the variance estimate

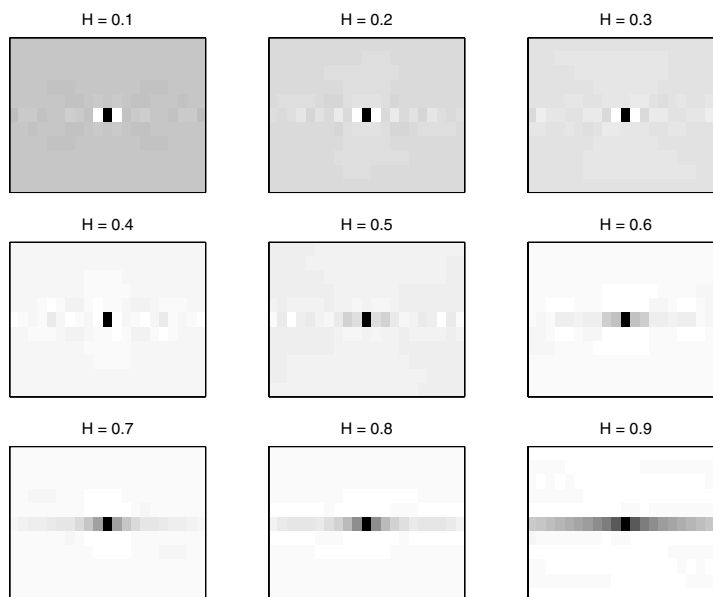


Fig. 11. Two-dimensional correlation function of the full IMF matrix, considered as a two-dimensional field, in the case of fractional Gaussian noise. For each value of the Hurst exponent H , the graph displays the quantity $|\hat{D}_H[k', n']|$ on a linear gray scale (from white for the minimum to black for the maximum). The horizontal (respectively, vertical) axis corresponds to time (respectively, IMF index) lags.

1 $\hat{V}_H[k]$ given in (3.14) is expected to be largely fluctuating, especially for large Hurst
 2 exponents H and large IMF indices k . Second, the negligible inter-scale correlations
 3 allows nevertheless for an estimation of the slope κ_H from a weighted linear regres-
 4 sion in the semi-log diagram $\log_2 \hat{V}_H[k]$ versus k . As far as the variability of the
 5 variance estimate is concerned, Fig. 9 gave a rough, second-order, indication on
 6 the basis of the observed standard deviation. A more complete appreciation can
 7 be gained from Fig. 12 where, in three typical cases ($H = 0.2, 0.5$ and 0.8), the
 8 experimental mean, median and various confidence intervals have been reported,
 9 together with the fitted model deduced from (3.13) as:

$$\log_2 V_H[k] = \log_2 \hat{V}_H[2] + 2(H - 1)(k - 2) \log_2 \rho_H \quad (3.20)$$

11 for $k \geq 2$. This series of simulations (which has been carried out on 10000 real-
 12 izations of 2048 data points in each case) evidences larger and larger fluctuations
 13 for modes of larger and larger indices, in agreement with (and generalization of)
 14 the findings reported in Ref. 15 for the only case of white noise. Moreover, the
 15 skewed (marginal) distribution of these “modegrams” reveal a better agreement
 16 when fitting the linear model (3.20) with the median rather than the mean of the
 17 realizations.

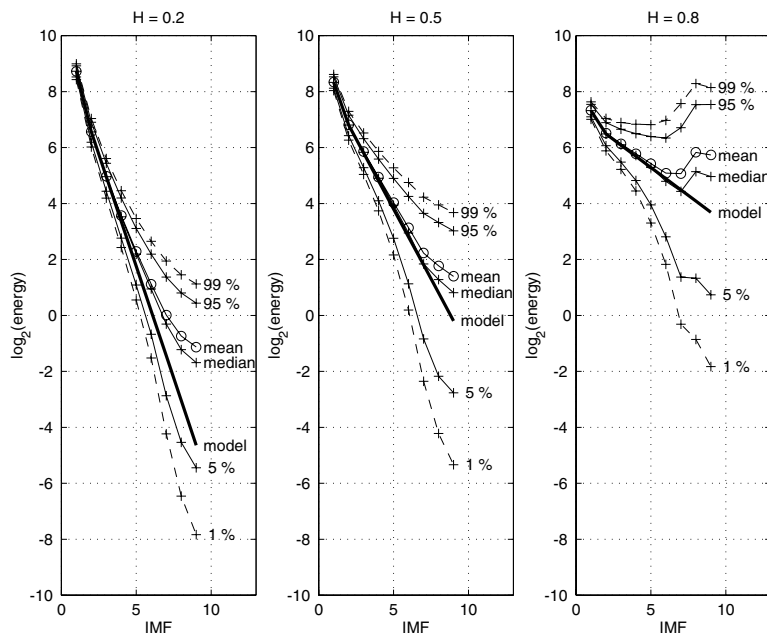


Fig. 12. Experimental “modegrams” in the case of fractional Gaussian noise. For the three considered values of the Hurst exponent, statistical characteristics (mean, median, confidence intervals) of the logarithm of the estimated EMD variance have been plotted as a function of the IMF index, together with the linear model given by (3.20).

Table 2. EMD versus wavelets (Daubechies 4): estimation of the Hurst exponent H in the case of fractional Gaussian noise.

H	0.1	0.2	0.3	0.4	0.5	0.6	0.7	0.8	0.9
\hat{H}_{EMD}	0.253	0.310	0.367	0.441	0.521	0.612	0.697	0.798	0.898
σ_{EMD}	0.070	0.072	0.070	0.075	0.074	0.074	0.079	0.081	0.091
\hat{H}_{W}	-0.071	0.117	0.261	0.386	0.502	0.610	0.715	0.819	0.920
σ_{W}	0.054	0.052	0.054	0.054	0.052	0.052	0.052	0.052	0.052

Table 3. EMD versus wavelets (Daubechies 4): estimation of the Hurst exponent H in the case of fractional Gaussian noise superimposed to a cubic trend.

H	0.1	0.2	0.3	0.4	0.5	0.6	0.7	0.8	0.9
\hat{H}_{EMD}	0.297	0.347	0.399	0.467	0.541	0.626	0.711	0.809	0.908
σ_{EMD}	0.074	0.073	0.073	0.079	0.077	0.079	0.082	0.085	0.094
\hat{H}_{W}	-0.071	0.117	0.261	0.386	0.502	0.610	0.715	0.819	0.920
σ_{W}	0.054	0.052	0.054	0.054	0.052	0.052	0.052	0.052	0.052

1 A quantitative comparison has been carried out between EMD and wavelets
 2 (Daubechies 4 in the present case), based on a data set of $J = 1000$ realizations of
 3 $N = 1024$ points each. The result, given in Table 2, shows that the two procedures
 4 behave quite the same (with respect to mean and standard deviation), with an
 5 equal difficulty for dealing with small values of H in the case of data with a small
 6 number of samples.

7 Finally, a second series of experiments has been carried out on the very same
 8 data set $\{x_H^{(j)}[n]; j = 1, \dots, J\}$, after superimposition of a cubic trend according to:

9
$$y_H^{(j)}[n] := \frac{x_H^{(j)}[n]}{\sqrt{\text{var } x_H}} + 20 \left(\frac{n}{N} - \frac{1}{2} \right)^3, \quad n = 1, \dots, N. \quad (3.21)$$

10 As is well-known, the number of vanishing moments $N_\psi = 4$ of the used wavelet
 11 is high enough to guarantee that the wavelet decomposition is following the super-
 12 imposed cubic trend,¹ and this can be checked by comparing the last two lines of
 13 Tables 2 and 3. As far as EMD is concerned, the trend is mostly captured by the
 14 residual, i.e. the IMF of largest index. Estimating therefore H from the first 6 IMFs
 15 only ends up with almost identical performance as compared to the no trend situ-
 16 ation, up to a slight increase in bias (due to the corruption by the trend at higher
 17 indices) and variance (due to the use of less IMFs).

4. Conclusion

18 By construction, EMD is based on no *a priori* filtering (even in a wide sense),
 19 but it rather selects, in a local, automatic and fully data-driven way, the “nat-
 20 ural” scales at which a signal oscillates. When applied to stationary broadband
 21 processes, the main conclusion of the study reported here is that EMD achieves

1 a decomposition on “intrinsic” modes (the so-called IMFs) whose effective spec-
 3 tra spontaneously organize as a constant- Q dyadic, wavelet-like, filter bank. This
 5 striking property has received here a detailed statistical analysis which, however,
 7 could be complemented by companion studies operating, e.g., in the time domain
 9 (equivalent impulse response⁷) rather than in the frequency domain. Whatever
 the domain considered for characterization, empirical findings about the statistics
 of EMD in well-controlled situations is the pre-requisite for a possible use of the
 method in processing tasks such as, e.g., denoising (in the spirit of Wu’s study¹⁵)
 or detrending.⁸

From a different perspective, the analysis has been carried out in a large, but
 specific, class of broadband stochastic processes, namely fractional Gaussian noise.
 It would be worth following the present investigations in the case of less regular
 models involving, e.g., mixtures of broadband and narrowband contributions. This
 is currently under investigation and will be presented in forthcoming publications.

15 Acknowledgments

The authors gratefully acknowledge Gabriel Rilling (ENS Lyon) for his help in the
 17 development of the Matlab codes, and his contribution to the initial studies on the
 EMD of fGn.

19 References

- 21 1. P. Abry, P. Flandrin, M. Taqqu and D. Veitch, Wavelets for the analysis, estima-
 23 tion, and synthesis of scaling data, in *Self-Similar Network Traffic and Performance
 Evaluation*, eds. K. Park and W. Willinger (Wiley, 2000), pp. 39–88.
- 25 2. K. T. Coughlin and K. K. Tung, 11-year solar cycle in the stratosphere extracted by
 27 the empirical mode decomposition method, *Adv. Space Res.*, Nov. 2002 (submitted).
- 29 3. N. E. Huang, Z. Shen, S. R. Long, M. L. Wu, H. H. Shih, Q. Zheng, N. C. Yen,
 C. C. Tung and H. H. Liu, The empirical mode decomposition and Hilbert spectrum
 for nonlinear and non-stationary time series analysis, *Proc. Roy. Soc. London* **A454**
 (1998) 903–995.
- 31 4. P. Embrechts and M. Maejima, *Selfsimilar Processes* (Princeton Univ. Press, 2002).
- 33 5. P. Flandrin, *Time-Frequency/Time-Scale Analysis* (Academic Press, 1999).
- 35 6. P. Flandrin, G. Rilling and P. Gonçalvès, Empirical mode decomposition as a filter
 bank, *IEEE Sig. Proc. Lett.*, 2004 (in press).
- 37 7. P. Flandrin and P. Gonçalvès, Sur la décomposition modale empirique, in *Proc. Coll.
 39 GRETSI sur le Traitement du Signal et des Images*, Vol. 1, Paris, 2003, pp. 149–152.
- 41 8. P. Flandrin and P. Gonçalvès, Denoising and detrending with Empirical Mode Decom-
 positions, in preparation.
9. R. Fournier, Analyse stochastique modale du signal stabilométrique. Application à
 l’étude de l’équilibre chez l’Homme, Thèse de Doctorat, University Paris XII Val de
 Marne, 2002.
10. S. Mallat, *A Wavelet Tour of Signal Processing* (Academic Press, 1998).
11. B. B. Mandelbrot and J. W. van Ness, Fractional Brownian motions, fractional noises
 and applications, *SIAM Rev.* **10** (1968) 422–437.

20 *P. Flandrin & P. Gonçalves*

- 1 12. G. Rilling, P. Flandrin and P. Gonçalves, On Empirical Mode Decomposition and its
3 algorithms, in *IEEE-EURASIP Workshop on Nonlinear Signal and Image Processing*
NSIP-03, Grado (I), 2003.
- 5 13. E. P. Souza Neto, M. A. Custaud, C. J. Cejka, P. Abry, J. Frutoso, C. Gharib
7 and P. Flandrin, Assessment of cardiovascular autonomic control by the Empirical
Mode Decomposition, in *4th Int. Workshop on Biosignal Interpretation*, Como (I),
9 pp. 123–126, 2002.
- 11 14. A. T. Wood and G. Chan, Simulation of stationary processes in $[0, 1]^d$, *J. Comp.*
13 *Graph. Stat.* **3** (1994) 409–432.
- 15 15. Z. Wu and N. E. Huang, A study of the characteristics of white noise using the
Empirical Mode Decomposition method, *Proc. Roy. Soc. London A*, December 2002
(submitted).
16. Z. Wu, E. K. Schneider, Z. Z. Hu and L. Cao, The impact of global warming on ENSO
variability in climate records, COLA Technical Report, CTR 110, October 2001.
17. <http://perso.ens-lyon.fr/patrick.flandrin/emd.html>